Ceramics International 44 (2018) 22370–22377

Contents lists available at ScienceDirect

Ceramics International

journal homepage: www.elsevier.com/locate/ceramint

3D gel-printing of Sr ferrite parts

Fang Yang[a,*], Xinyue Zhang[a], Zhimeng Guo[a,*], Alex A. Volinsky[b]

[a] Institute for Advanced Materials and Technology, University of Science and Technology Beijing, Beijing 100083, China
[b] Department of Mechanical Engineering, University of South Florida, Tampa, FL 33620, USA

ARTICLE INFO

Keywords:
3D printing
Sr ferrite
Gelation
Ceramic slurry

ABSTRACT

3D gel-printing (3DGP) opens new possibilities to process complex-shaped Sr ferrite parts for magnetic applications. In this study, a novel 3DGP process based on the hydroxyethyl methacrylate gelation system was employed to prepare complex-shaped Sr ferrite samples. To obtain highly loaded pseudo-plastic slurries, the Sr ferrite powder was modified by 1 wt% silane coupling agent and 2.5 vol% polymer Silok7050S was introduced into the ceramic slurry as a dispersant. In the printed samples, good dimensional accuracy and surface quality were achieved with a relatively low surface roughness of 5 μm. After sintering, the Sr ferrite ceramics exhibited good surface quality and the surface roughness was 3.2 μm. A homogeneous microstructure was observed. The bending strength for the sintered samples with the relative density of 97% was 83 MPa. In addition, the corresponding coercivity, remanence, and maximum magnetic energy product values were 271.2 kA/m, 0.383 T, and 26.34 kJ/m^3, respectively.

1. Introduction

Sr ferrite was developed in the 1950s by the scientists at Philips Laboratories [1,2]. Due to its distinct magnetic properties, such as high Curie temperature, magnetization, permeability, and coercivity, along with excellent chemical stability, corrosion resistivity, and low production cost [3–5], it has been widely used in industrial applications, such as rotors in brushless DC electric motors [6]. Nowadays, the trend for downsizing electronic devices with complex shapes has led to the demand for promising technology to obtain the desirable Sr ferrite parts [7,8]. Recently, the application of powder injection molding (PIM) has been reported for fabricating complex-shaped sintered Sr ferrite ceramics [9]. PIM is of interest since it offers the potential for the production of complex-shaped parts [10]. Nevertheless, there are still some drawbacks to PIM, such as specific tooling requirements for injection molding [11].

Additive manufacturing (AM) has received much attention because of the flexible manufacturing ability to translate the complex-shaped geometries directly into 3D objects [12,13]. Its main benefits include freedom of design, mass customization, waste minimization and the ability to manufacture complex structures [14,15]. Typical AM technologies include three-dimensional printing (3DP) [16], selective laser melting (SLM) [17], selective laser sintering (SLS) [18], stereolithography (SLA) [19], fused deposition molding (FDM) [20], electron beam melting (EBM) [21], and direct inkjet printing (DIP) [22]. Owing to the unique fabrication method, AM is well-suited to fabricate complex-shaped parts. To date, the majority of the additive manufacturing efforts have been carried out to print fiber-reinforced composites [23], rechargeable micro-batteries [24], structural metals [25], and high-temperature ceramics [26]. Nevertheless, AM printing of Sr ferrite ceramics is still in its infancy.

Generally, 3DP, SLA, and DIP were employed to produce ceramic parts. However, relatively low solid loading of the ceramic slurry of typically less than 40 vol% was the main obstacle for the AM printing process [27]. Very recently, 3D gel-printing (3DGP) based on gel-casting was proposed for producing complex-shaped parts with highly loaded printing slurry [28]. Gel-casting is an attractive near-net-shaped colloidal forming technique with the high solid loading of suspensions, including harsh crosslinking polymers or curing agents [29,30]. With the combination of gel-casting and 3D printing, 3DGP is a promising method to enable miniaturization of complex-shaped Sr ferrite parts.

Therefore, it is of interest to employ 3DGP to fabricate Sr ferrite ceramics. To date, no related reports have been presented regarding this topic. In this paper, a highly loaded pseudo-plastic printing slurry was prepared to print Sr ferrite ceramics. The slurry preparation, 3D printing, and sintering of 3DGP Sr ferrite ceramics were investigated.

* Corresponding authors.
E-mail addresses: yangfang@ustb.edu.cn (F. Yang), zmguo@ustb.edu.cn (Z. Guo).

https://doi.org/10.1016/j.ceramint.2018.08.364
Received 21 August 2018; Received in revised form 31 August 2018; Accepted 31 August 2018
Available online 01 September 2018

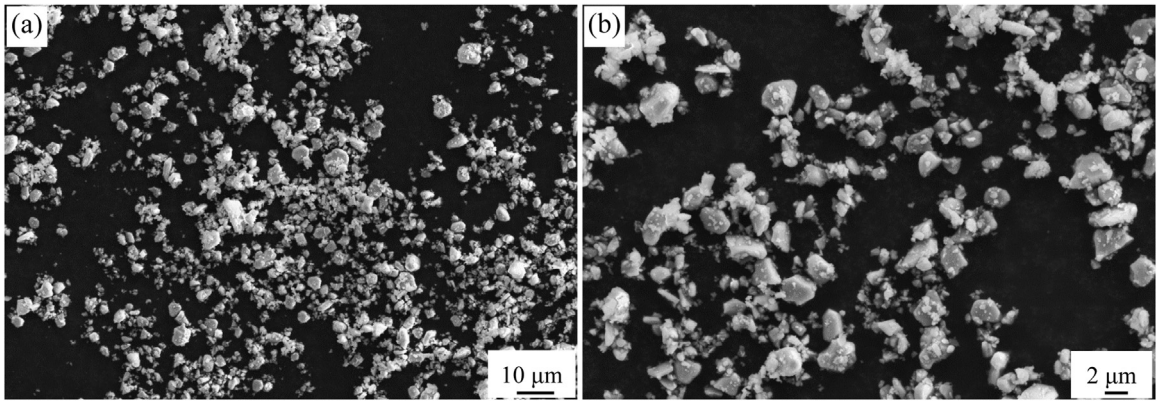

Fig. 1. SEM images of raw Sr ferrite powders: (a) low and (b) high magnification.

2. Experimental procedure

2.1. Slurry preparation

Commercial Sr ferrite powder (China Grirem Advanced Materials Co., Ltd) with a mean particle size of 1 μm was used as raw material. Fig. 1 shows the morphology and the particle size distribution of Sr ferrite powders. First, the Sr ferrite powders were treated with silane coupling agent KH560 (AR, Sinopharm Chemical Reagent Co., Ltd) to improve the surface activity of powders. Second, hydroxyethyl methacrylate monomer (HEMA, AR, Sinopharm Chemical Reagent Co., Ltd) and N, N′-methylenebisacrylamide as crosslinker (MBAM, AR, Sinopharm Chemical Reagent Co., Ltd) were added into deionized water. Then, polymer Silok7050S (AR, Guangzhou Siloky Chemical Reagent Co., Ltd) was added as a dispersant into the mixture to produce a premixed solution. Finally, to obtain the printing slurry, modified Sr ferrite powder was added into the premixed solution and mixed in a planetary centrifugal mixer at atmospheric pressure for 30 min Table 1 lists the composition of the raw materials.

2.2. 3D printing

Fig. 2 shows the schematic diagram of the 3DGP method for printing Sr ferrite parts. At the start of printing, 3D models were designed and sliced into the printing code. Second, the printing slurry was loaded into a plastic syringe barrel with a nozzle. A solution with N, N, N′, N′-tetramethylethylenediamine (TEMED, AR, Sinopharm Chemical Reagent Co., Ltd) as a catalyst and ammonium persulphate (APS, AR, Sinopharm Chemical Reagent Co., Ltd) as an initiator was delivered to the screw extruder along with the slurry to adjust the gelation time. Then, the nozzle continuously printed Sr ferrite parts at a speed of 20 mm/s. The stage motion was controlled by the computer system. After the 3DGP process, the printed green samples were dried in a vacuum oven at 50 °C for 8 h. The dried green samples were treated at 500 °C for 1 h and then sintered at 1300 °C for 2 h with a heating rate of 4 °C/min in a tube furnace under an argon atmosphere. Subsequently, the sintered samples were performed furnace cooling to room temperature.

Table 1
Composition of the raw materials.

Raw materials	Content (vol%)
Sr ferrite powder	50
HEMA	9.1
MBAM	0.76
Silok7050S	0.25
TEMED	0.4
APS	0.32
Water	Bal.

2.3. Tests and characterization

The viscosity of the Sr ferrite slurry was tested by a rotational viscometer (Brookfield LYDV-S). The density of the sintered magnets was determined by the Archimedes' type measurements. Five samples for each processing condition were tested to confirm reproducibility. The room temperature magnetic properties were measured by a magnetic measurement device (NIM-200C). The transverse rupture strength (TRS) of the sintered samples was tested by the three-point bending using an electronic universal testing machine (Instron CMT 4305). The surface roughness and morphology of the printed and sintered magnets were measured by a confocal laser scanning microscope (CLSM, OLYMPUS LEXT OLS4100). Microstructure and fracture surfaces were characterized by field emission scanning electron microscopy (FESEM, Supra55).

3. Results and discussion

3.1. Sr ferrite slurry preparation

Low viscosity with high solid loading is the main parameter for the printing slurry. Fig. 3 shows the viscosity of printing slurry without dispersant as a function of solid loading. Sr ferrite powders were dispersed in the solution, which consisted of HEMA, MBAM, and deionized water. As shown in Fig. 3, the slurry viscosity increased with the solid loading. When the solid loading reached 50 vol%, the corresponding slurry viscosity was about 13.5 Pa s, which was much higher than the ideal viscosity value for printing. To obtain printed green samples with high quality, the viscosity should be lower than 3 Pa s. It was often difficult to obtain a highly loaded slurry with low viscosity, especially for fine Sr ferrite powders.

To reduce the slurry viscosity, different dispersants were introduced into the slurry. Normally, ammonium citrate (AC) is used as a typical dispersant in gelatin systems. However, for the Sr ferrite slurry, there were no notable changes in the viscosity with AC addition. First, the viscosity significantly decreased and then increased with the Silok7050S dispersant content, as shown in Fig. 4(a). The optimal content of Silok7050S was 0.25 vol%. With the 0.25 vol% Silok7050S addition, the viscosity decreased from 13.5 Pa s to 7.3 Pa s. At this point, a high coverage of particles without bridging was achieved and the stable dispersion of powders in the slurry was supported by high electrostatic repulsive interactions. At relatively low Silok7050S

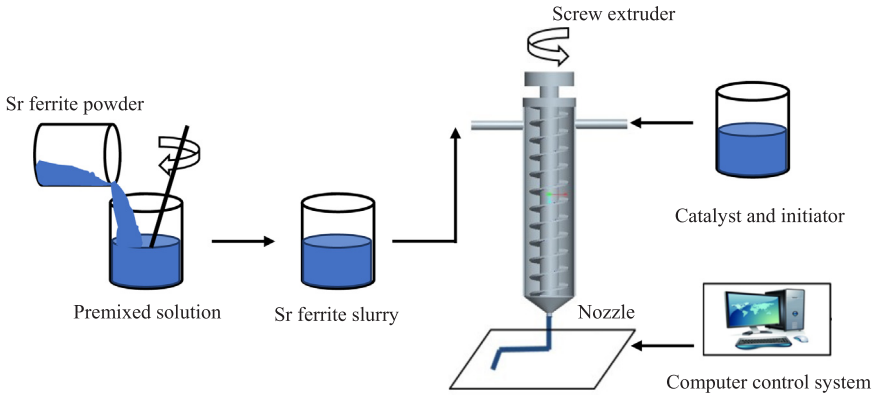

Fig. 2. Schematic diagram of the 3DGP process for printing Sr ferrite parts.

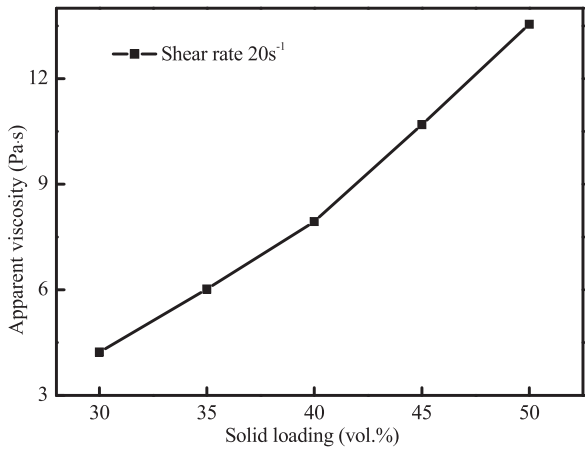

Fig. 3. The viscosity of printing slurry without dispersant as a function of solid loading.

content, since some particles were not covered with the polymer, they were in direct contact with other particles and formed aggregates, increasing the slurry viscosity. With excess dispersant addition, polymer bridge formed between primary particles, resulting in the acceleration of powder aggregation and viscosity increase [31].

Similarly, silane coupling agent was employed to modify the Sr ferrite powder. First, Sr ferrite powders were mixed with various amounts of silane (0, 0.5, 1.0, 1.5, 2 wt%). Second, a solution of deionized water and alcohol at a volume ratio of 1:1 was added into the mixed powders, just enough to immerse the powder. Then, the suspension was mixed in a planetary centrifugal mixer for 24 h. After drying, the modified Sr ferrite powders were obtained with a silane coating. The viscosity change with silane coating is shown in Fig. 4(b). The viscosity decreased first and then increased with the silane content. Furthermore, 1 wt% was considered the best silane content. The alkoxy groups (OCH_3) of the silane were transformed into silanol (Si-OH) during the hydrolysis in the aqueous media, as shown in reaction (1) [32]. Thereafter, the Si-OH was coated on the surface of Sr ferrite powder (reaction (2)), which was beneficial to improve the powder surface activity, resulting in enhanced slurry fluidity. The coupling agent enhanced the consistency of the inorganic powders and the polymer and the dispersion of inorganic powders in the polymer.

$$CH_2OCHCH_2O(CH_2)_3Si(OCH_3)_3+3H_2O \rightarrow CH_2OCHCH_2O(CH_2)_3Si(OH)_3 +3CH_3OH \quad (1)$$

$$Si-OH+\bullet(\text{Sr ferrite particle}) \rightarrow \bullet-Si-OH \quad (2)$$

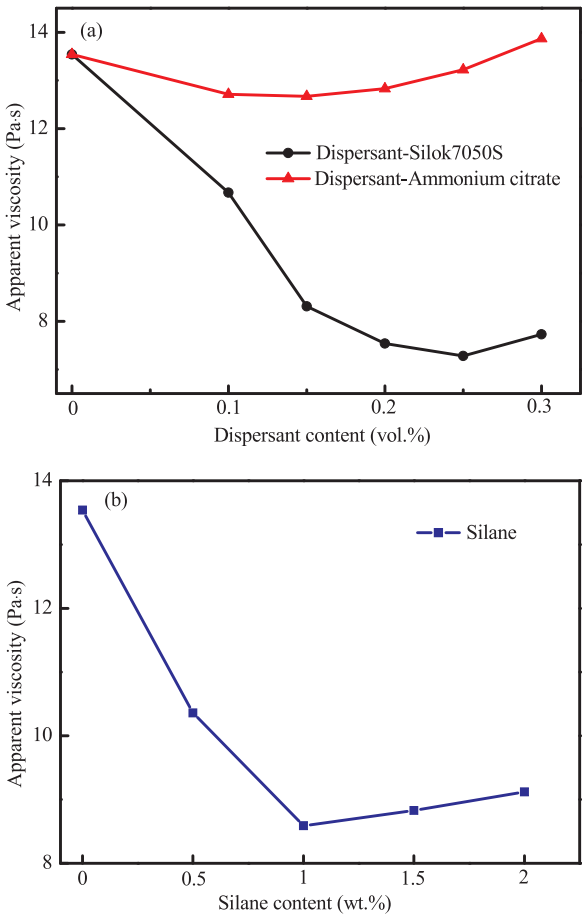

Fig. 4. The viscosity of 50 vol% Sr ferrite slurry as a function of (a) dispersant, and (b) silane content.

Consequently, modified Sr ferrite powder coated with 1 wt% silane was added into the premixed solution. Fig. 5 shows the viscosity of 50 vol% Sr ferrite slurry with 1 wt% silane as a function of dispersant content. The viscosity decreased to 1.96 Pa s with the 0.25 vol% Silok7050S addition, which was much lower than 3 Pa s. Slurry with pseudoplastic behavior is highly desirable for controlling the forming shape. The rheological curve of the slurry is shown in Fig. 6. The viscosity decreased with the shear rate and reached a stable state at the shear rate above 200 s^{-1}. The slurry shows a shear-shinning behavior, indicating that it is suitable for the 3DGP printing.

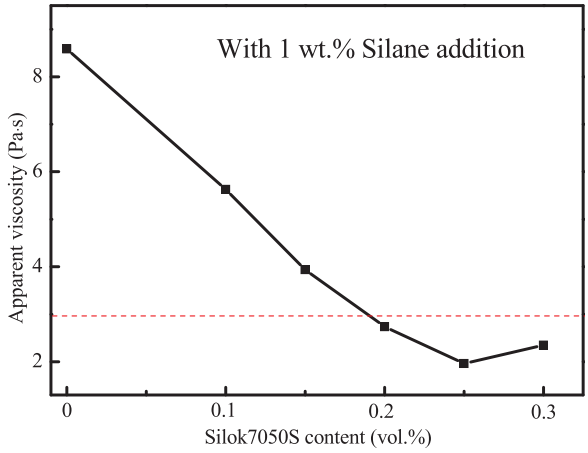

Fig. 5. The viscosity of 50 vol% Sr ferrite slurry with 1 wt% silane addition as a function of dispersant content.

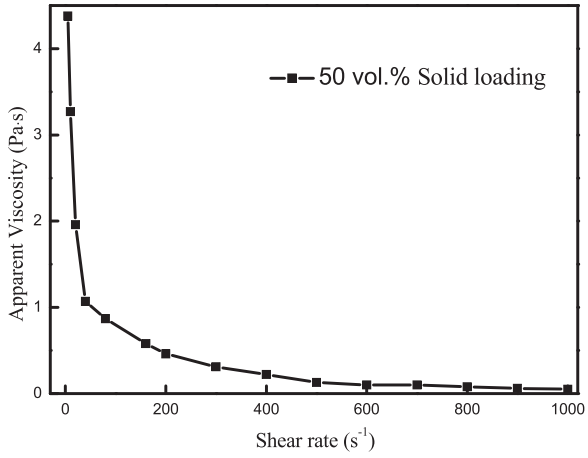

Fig. 6. The viscosity of 50 vol% Sr ferrite slurry as a function of the shear rate.

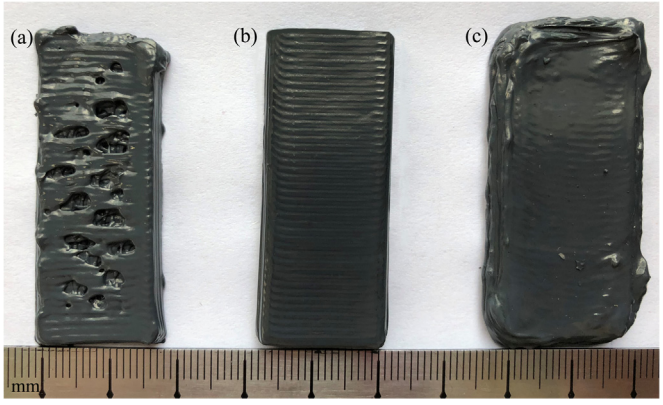

Fig. 7. Green samples printed by 3DGP with the extrusion rate of: (a) 1 cm^3/min, (b) 1.5 cm^3/min, and (c) 2 cm^3/min.

Table 2
Printing parameters for the printed Sr ferrite parts.

Printing parameter	Value
Layer height	0.2 mm
Nozzle diameter	0.5 mm
Printer speed	20 mm/s
Fill density	95%
Extrusion rate	1.5 cm^3/min
Bed temp.	25 °C

3.2. Printing of the slurry

The slurry was extruded from the nozzle under the application of air pressure. Thereinto, the extrusion rate, printing speed, layer height and nozzle diameter are the key factors for the printing quality. Although the high printing speed can significantly improve manufacturing efficiency, it is required to be matched with the extrusion rate. As shown in Fig. 7(a), discontinuous printing trajectory was observed in the printed sample with existing bulges and pits. The extrusion rate of 1 cm^3/min was relatively low. When the extrusion rate was increased to 2 cm^3/min, low dimensional accuracy and poor surface quality were observed in the printed sample. Printed lines overlapped and even collapsed, as shown in Fig. 7(c). The printing slurry cannot solidify in time to maintain the designed shape. The optimal extrusion rate for the Sr ferrite ceramic slurry was 1.5 cm^3/min. The printed sample had good dimensional accuracy and surface quality, as shown in Fig. 7(b). Meanwhile, the printing speed and layer height also have the same effects on the printing quality. The optimal printing parameters for the 3DGP Sr ferrite samples printed with high accuracy are listed in Table 2.

A rectangular block as an example was printed by the 3DGP process, as shown in Fig. 8(a). The printed lines were observed, while there were no defects or deformation on the surface, as shown in Fig. 8(b), which illustrated that the ceramic slurry was suitable for printing. The printed lines can be obviously observed. The width between the adjacent two printed lines was 0.53 mm, which is close to the nozzle diameter. The top surface was homogenous. The surface roughness of the printed sample was about 5 μm, as shown in Fig. 8(c). After extrusion and deposition on the print platform, the shape of the printed slurry lines changed from cylindrical to elliptic cylindrical because of the slurry weight and rheological behavior, and the slurry spread out to fill the spaces between the printed lines before gelation.

The gelation process based on the HEMA monomer free radical polymerization generally consisted of three elementary reactions-chain initiations, chain propagation and chain termination [33]. First, the initiator (APS) decomposed to generate free radicals, as shown in reaction (3). Then, monomer radicals were generated by the additional reaction of HEMA and free radicals, following reaction (4). After that, the monomer radicals continuously combined HEMA monomer to generate chain-free radicals. Monomer radicals can polymerize with each other to form chain structures of macromolecules, as shown in reaction (5), where R is 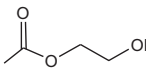 . Last, due to the loss of activity of free radicals, chains stopped growing. Stable chains of polymer molecules were formed to bind Se ferrite particles together.

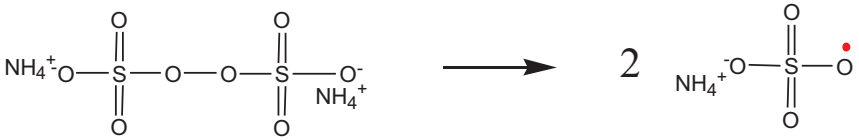

(3).

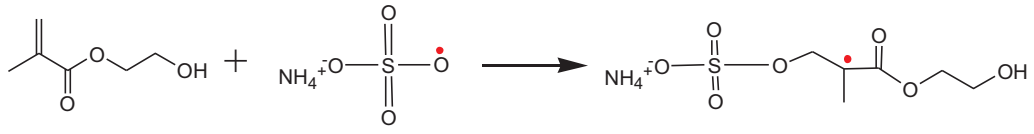

(4).

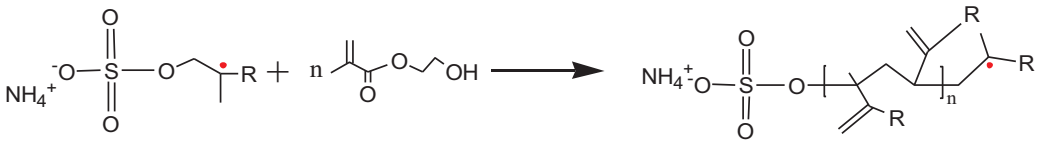

(5).

Accordingly, the bending strength of the 3DGP green samples was about 18 ± 0.8 MPa. Fig. 9 shows the fracture morphology of the printed sample. After gelation, fine Sr ferrite particles were closely bound under the action of the organic binder. The interfaces between the printed layers and lines cannot be observed. In addition, Sr ferrite particles were uniformly distributed in the printed sample.

3.3. Sintering of the printed sample

Fig. 10 shows the appearance, surface morphology and surface roughness of the as-sintered block sample prepared by 3DGP. The as-sintered sample has good surface quality with no observed defects or deformation, indicating that the printed sample uniformly shrank during sintering. The distance between two adjacent lines was 0.42 mm, which is narrower than in the as-printed sample. Meanwhile, the surface roughness of the sintered sample decreased to 3.2 μm, as shown in Fig. 10(c), while the roughness for the as-printed sample was 5 μm. It can be inferred that the surface quality of the as-printed sample can be improved after sintering, which was consistent with the results shown in Fig. 11. Clear and obvious printing lines can be observed on the top surface of the sintered sample, without defects or pores. The printing trajectory can be visible from the cross-section of the sample in Fig. 11(b). Overall, the sintered sample had a homogeneous microstructure.

After sintering at 1300 °C for 2 h, the density for the sintered ceramics was about 5.34 g/cm^3, which is nearly 97% dense compared to the theoretical density of 5.5 g/cm^3. In addition, the average bending strength for the Sr ferrite ceramic was about 83 ± 2 MPa. The corresponding fracture morphology is shown in Fig. 12. A typically brittle fracture was observed. Sr ferrite particles were packed uniformly without any large defects and slender polymer chains can be observed connecting the particles, which were responsible for the high strength of the green body. The fracture surface of the sintered ceramics exhibited a homogenous microstructure, as shown in Fig. 12(b). However, the sintered ceramics had a relative density of 97%, which indicated that some micropores still existed even in the sintered sample.

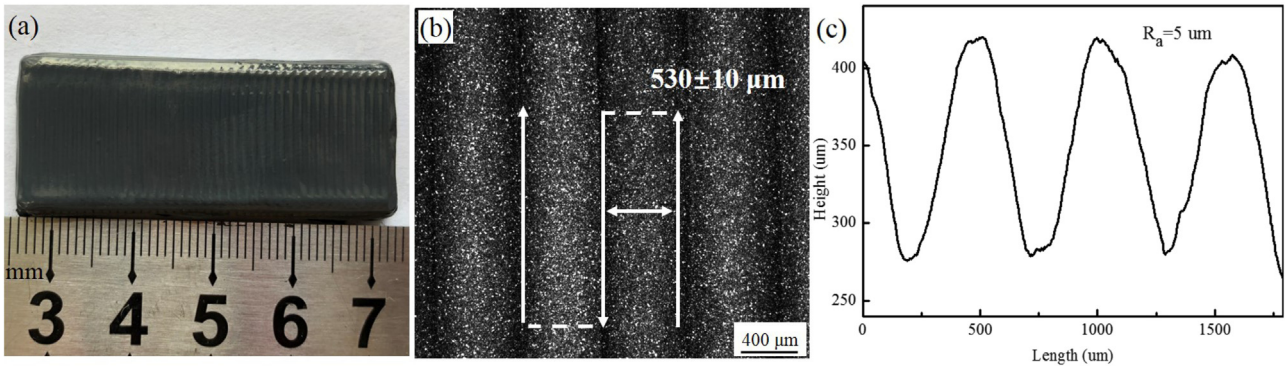

Fig. 8. The printed Sr ferrite sample: (a) printed rectangular block, (b) surface morphology, and (c) surface roughness.

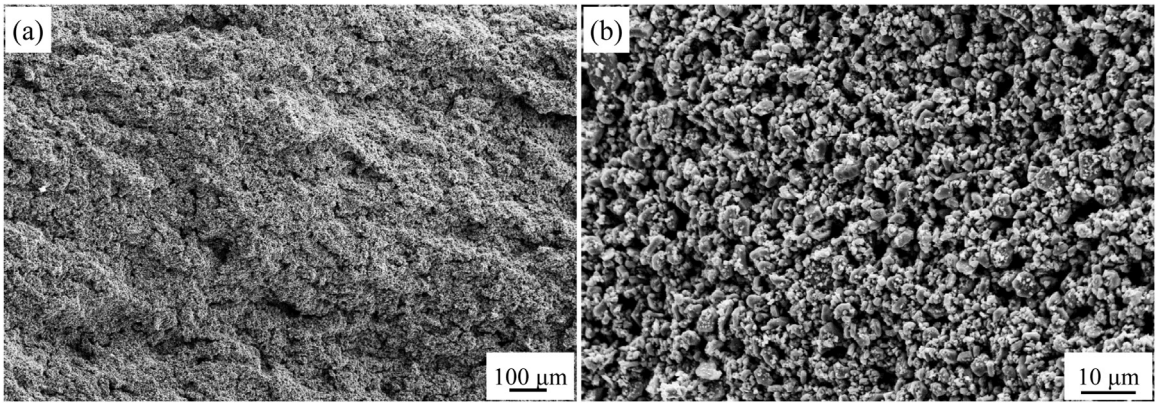

Fig. 9. The fracture morphology of the printed Sr ferrite sample: (a) low and (b) high magnification.

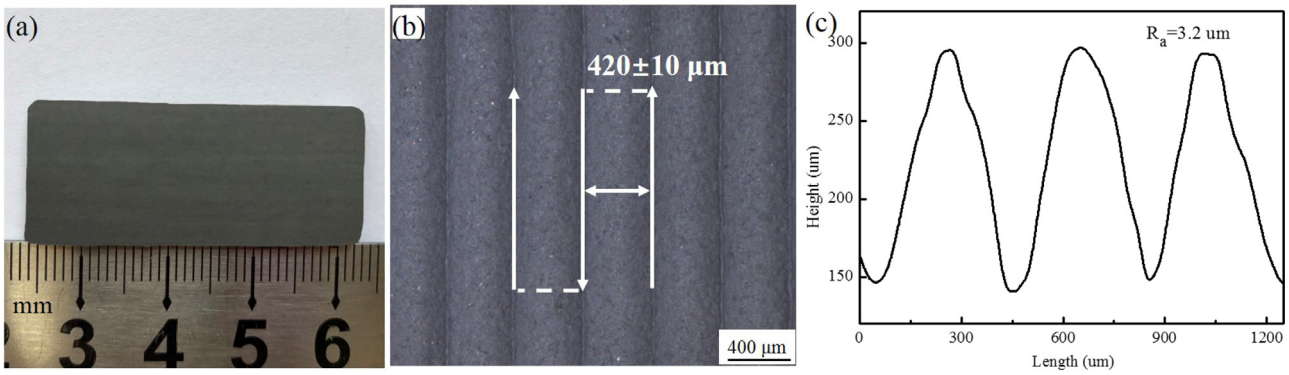

Fig. 10. The sintered Sr ferrite sample: (a) sintered rectangular block, (b) surface morphology, and (c) surface roughness.

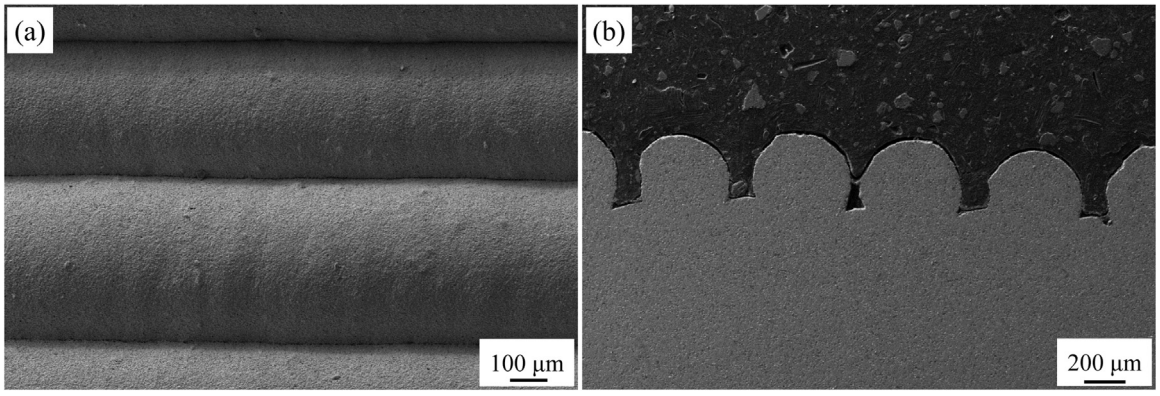

Fig. 11. SEM morphology of the sintered Sr ferrite sample: (a) top surface, (b) cross section.

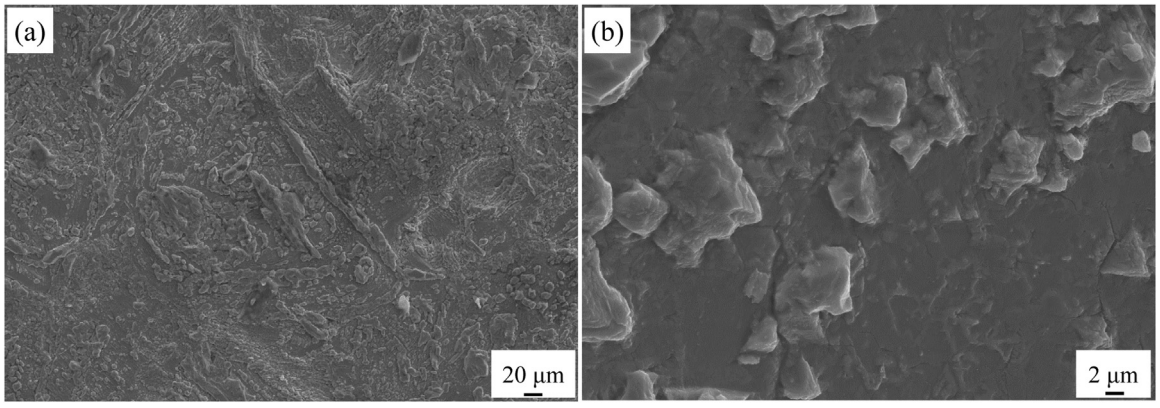

Fig. 12. The fracture morphology of the sintered Sr ferrite sample: (a) low and (b) high magnification.

Fig. 13 presents the magnetic properties of the sintered Sr ferrite sample prepared by 3DGP. The measured coercivity H_{cj}, remanence B_r and maximum magnetic energy product $(BH)_{max}$ values were 271.2 kA/m, 0.383 T, and 26.34 kJ/m^3, respectively. The characteristics of the Sr ferrite powder used were: H_{cj} = 263–295 kA/m, Br = 0.405–0.415 T, and $(BH)_{max}$ = 30.3–31.9 kJ/m^3. Overall, there was basically no degradation in the intrinsic coercivity in the as-sintered samples. However, there was little degradation in the remanence and maximum magnetic energy product. This may be related to incomplete densification of the sintered sample prepared by 3DGP. Therefore, improving the sintered density is the main focus of future research.

3.4. Complex-shaped parts

Fig. 14 shows several complex-shaped Sr ferrite ceramics prepared by the 3DGP process. The printed samples shrank uniformly during sintering. After sintering, the samples had good dimensional stability and surface quality, which implied that the 3DGP process can be employed to prepare near-net-shaped Sr ferrite ceramics. In actual production, if the shrinkage coefficient is known, complex shaped parts

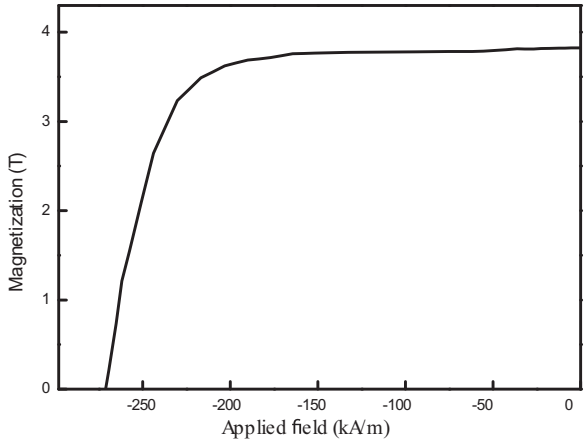

Fig. 13. Demagnetization curve for the as-sintered Sr ferrite magnets.

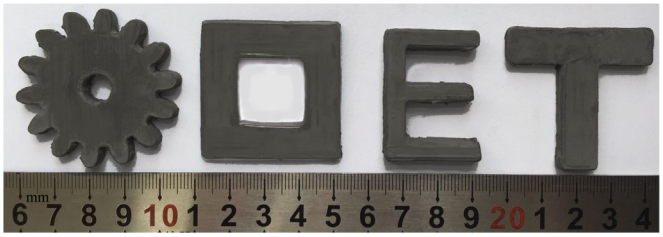

Fig. 14. The as-sintered Sr ferrite parts prepared by the 3DGP process.

with the desired size can be obtained by 3DGP. Combining the advantages of gel-casting with the 3D printing formability, 3DGP is an ideal route for preparing miniature complex-shaped Sr ferrite ceramic parts. In addition, it also unlocks the potential of complex shape designs and reduces post-manufacturing costs.

4. Conclusions

In this study, complex-shaped Sr ferrite ceramics were printed by the 3DGP process. With the modification of the slurry viscosity, highly loaded pseudo-plastic Sr ferrite slurries of 50 vol% were prepared with the HEMA-based gelation system. The gelation mechanism was explored. By optimizing the printing parameters, the printed samples with good surface quality were obtained. The corresponding surface roughness was 5 μm. Meanwhile, the sintered sample also exhibited good surface quality and the surface roughness was 3.2 μm. A homogeneous microstructure was observed in the sintered samples. The relative density and average bending strength of the sintered samples were 97% and 83 MPa, respectively. Besides, a comprehensive magnetic performance of the sintered 3DGP sample was obtained (H_{cj} = 271.2 kA/m, B_r = 0.383 T, and $(BH)_{max}$ = 26.34 kJ/m^3). Therefore, 3DGP is a promising method to prepare complex-shaped Sr ferrite parts.

Acknowledgments

This work was supported by the State Key Lab of Advanced Metals and Materials, China (No. 2018-Z06). AV acknowledges support from the National Science Foundation, United States (IRES 1358088).

References

[1] B. Abraime, M.A. Tamerd, A. Mahmoud, F. Boschini, A. Benyoussef, M. Hamedoun, Y. Xiao, A.E. Kenz, O. Mounkachi, Experimental and theoretical investigation of $SrFe_{12}O_{19}$ nanopowder for permanent magnet application, Ceram. Int. 43 (2017) 15999–16006, https://doi.org/10.1016/j.ceramint.2017.08.187.

[2] M. Stingaciu, M. Topole, P. Mcguiness, M. Christensen, Magnetic properties of ball-milled $SrFe_{12}O_{19}$ particles consolidated by spark-plasma sintering, Sci. Rep. 5 (2015) 14112, https://doi.org/10.1038/srep14112.

[3] A. Thakur, R.R. Singh, P./B. Barman, Synthesis and characterizations of Nd3+ doped $SrFe_{12}O_{19}$ nanoparticles, Mater. Chem. Phys. 141 (2013) 562–569, https://doi.org/10.1016/j.matchemphys.2013.05.063.

[4] C.C. Huang, A.H. Jiang, Y.H. Huang, C.H. Liou, Y.C. Wang, C.P. Lee, T.Y. Huang, C.C. Shaw, M.F. Kuo, C.H. Cheng, Influence of $CaCO_3$ and SiO_2 additives on magnetic peoperties of M-type Sr ferrites, J. Magn. Magn. Mater. 451 (2018) 288–294, https://doi.org/10.1016/j.jmmm.2017.09.070.

[5] C. Na, Y. Kai, M.Y. Gu, Microwave absorption properties of La-substituted M-type strontium ferrites, J. Alloy. Compd. 409 (2010) 609–612, https://doi.org/10.1016/j.jallcom.2009.10.116.

[6] C.C. Huang, Y.H. Hung, M.F. Kuo, Study of the effect of specific surface area and purity of Fe_2O_3 on the magnetic peoperties of Sr-hexaferrites, IEEE Trans. Magn. 52 (2016) 2101909, https://doi.org/10.1109/TMAG.2016.2518124.

[7] J. Gutierrez-Lopez, E. Rodriguez-Senin, J.Y. Pastor, M.A. Paris, A. Matrin, B. Levenfeld, A. Varez, Microstructure, magnetic and mechanical properties of Ni-Zn ferrites prepared by powder injection molding, Powder Technol. 210 (1) (2011) 29–35 (https://doi.org/j.powtec.2011.02.008).

[8] N. Murillo, J. Gonzalez, C. Guraya, M. Gutierrez, F.J. Seco, Structural and magnetci peoperties of sintered Sr-ferrites fabricated by powder injection molding, J. Magn. Magn. Mater. 203 (1999) 165–168, https://doi.org/10.1016/S0304-8853(99)00251-6.

[9] Y. Ye, L. Qiao, J.W. Zheng, Y. Ying, W.C. Li, J. Yu, S.L. Che, L.Q. Jiang, Effect of microcrystalline wax on the solvent debinding of Sr-ferrite ceramics prepared by powder injection molding, J. Eur. Ceram. Soc. 37 (2017) 2015–2114, https://doi.org/10.1016/j.jeurceramsoc.2016.12.026.

[10] I.D. Jung, S.H. Kim, S.J. Park, T.G. Kang, J.M. Park, Rheological modeling of strontium ferrite feedstock for magnetci powder injection molding, Powder Technol. 262 (2014) 198–202, https://doi.org/10.1016/j.powtec.2014.04.073.

[11] L. Li, A. Tirado, I.C. Nlebedim, O. Rios, B. Post, V. Kunc, R.R. Lowden, E. Lara-Curzio, R. Fredette, J. Ormerod, T.A. Lograsso, M.P. Paranthaman, Big area additive manufacturing of high performance bonded NdFeB magnets, Sci. Rep. 6 (2016) 36212, https://doi.org/10.1038/srep36212.

[12] S. Kumar, J.P. Kruth, Composites by rapid prototyping technology, Mater. Des. 31 (2010) 850–856, https://doi.org/10.1016/j.matdes.2009.07.045.

[13] L. Santana, J.L. Alves, A. da C.S. Netto, A study of parametric calibration for low cost 3D printing: seeking improvement in dimensional quality, Mater. Des. 135 (2017) 159–172, https://doi.org/10.1016/j.matdes.2017.09.020.

[14] M. Bodaghi, A.R. Damanpack, G.F. Hu, W.H. Liao, Large deformations of soft metamaterials fabricated by 3D printing, Mater. Des. 131 (2017) 81–91, https://doi.org/10.1016/j.matdes.2017.06.002.

[15] T.D. Ngo, A. Kashani, G. Imbalzano, K.T.Q. Nguyen, D. Hui, Additive manufacturing (3D printing): a review of materials, methods, applications and challenges, Compos. Part. B. Eng. 143 (2018) 172–196, https://doi.org/10.1016/j.compositesb.2018.02.012.

[16] E. Sachs, M. Cima, P. Williams, D. Brancazio, J. Cornie, Three dimensional printing: rapid tooling and prototypes directly from a CAD model, CIRP Ann. 39 (1990) 201–204, https://doi.org/10.1016/S0007-8506(07)61035-X.

[17] E. Chlebus, B. Kuźnicka, T. Kurzynowski, B. Dybała, Microstructure and mechanical behaviour of Ti-6Al-7Nb alloy produced by selective laser melting, Mater. Charact. 62 (2011) 488–495, https://doi.org/10.1016/j.matchar.2011.03.006.

[18] S.K. Tiwari, S. Pande, S. Agrawal, S.M. Bodade, Selection of selective laser sintering materials for different applications, Rapid Prototyp. J. 21 (2015) 630–648, https://doi.org/10.1108/RPJ-03-2013-0027.

[19] F.P.W. Melchels, J. Feijen, D.W. Grijpma, A review on stereolithography and its applications in biomedical engineering, Biomaterials 31 (2010) 6121–6130, https://doi.org/10.1016/j.biomaterials.2010.04.050.

[20] O.S. Carneiro, A.F. Silva, R. Gomes, Fused deposition modeling with polypropylene, Mater. Des. 83 (2015) 768–776, https://doi.org/10.1016/j.matdes.2015.06.053.

[21] D. Cormier, O. Harrysson, H. West, Characterization of H13 steel produced via electron beam melting, Rapid Prototyp. J. 10 (2004) 35–41, https://doi.org/10.1108/13552540410512516.

[22] M. Bissannagari, J. Kim, Inkjet printing of NiZn-ferrite films and their magnetic properties, Ceram. Int. 41 (2015) 8023–8027, https://doi.org/10.1016/j.ceramint.2015.02.151.

[23] B.G. Compton, J.A. Lewis, 3D-printing of lightweight cellular composites, Adv. Mater. 26 (2014) 5930–5935, https://doi.org/10.1002/adma.201401804.

[24] K. Sun, T.S. Wei, B.Y. Ahn, J.Y. Seo, S.J. Dillon, J.A. Lewis, 3D printing of interdigitated li-Ion microbattery architectures, Adv. Mater. 25 (2013) 4539–4543, https://doi.org/10.1002/adma.201301036.

[25] A.E. Jakus, S.L. Taylor, N.R. Geisendorfer, D.C. Dunand, R.N. Shah, Metallic architectures from 3D-printed powder-based liquid inks, Adv. Funct. Mater. 25 (2015) 6985–6995, https://doi.org/10.1002/adfm.201503921.

[26] S.L. Morissette, J.A. Lewis, J. Cesarano, D.B. Dimos, T.Y. Baer, Solid freeform fabricaction of aqueous alumina-poly(vinylalcohol) gelcasting suspensions, J. Am. Ceram. Soc. 83 (2000) 2409–2416, https://doi.org/10.1111/j.1151-2916.2000.tb01569.x.

[27] H.P. Shao, D.C. Zhao, T. Lin, J.Z. He, J. Wu, 3D gel-printing of zirconia ceramic parts, Ceram. Int. 43 (2017) 13939–13942, https://doi.org/10.1016/J.CERAMINT.2017.07.124.

[28] X.Y. Zhang, Z.M. Guo, C.G. Chen, W.W. Yang, Additive manufacturing of WC-20Co components by 3D gel-printing, Int. J. Refract. Met. Hard 70 (2017) 215–223, https://doi.org/10.1016/j.ijrmhm.2017.10.005.

[29] K. Cai, Y. Huang, J.L. Yang, Alumina gelcasting by using HEMA system, J. Eur. Ceram. Soc. 25 (2005) 1089–1093, https://doi.org/10.1016/j.jeurceramsoc.2004.04.024.

[30] R. Xie, D. Zhang, X.Y. Zhang, K.C. Zhou, T.W. Button, Gelcasting of alumina ceramics with improved green strength, Ceram. Int. 38 (2012) 6923–6926, https://doi.org/10.1916/j.ceramint.2012.05.027.
[31] Y. Fukuda, T. Togahi, Y. Suzuki, M. Naito, H. Kamiya, Influence of additive content of anionic polymer dispersant on dense alumina suspension viscosity, Chem. Eng. Sci. 56 (2001) 3005–3010, https://doi.org/10.1016/S0009-2509(00)00483-8.
[32] S. Akhtar, A. Matin, A.M. Kumar, A. Ibrahim, T. Laoui, Enhancement of anticorrosion property of 304 stainless steel using silane coatings, Appl. Surf. Sci. 440 (2018) 1286–1297, https://doi.org/10.1016/j.apsusc.2018.01.203.
[33] X.Y. Ren, H.P. Shao, T. Lin, H. Zheng, 3D gel-printing-an additive manufacturing method for producing complex shape parts, Mater. Des. 101 (2016) 80–87, https://doi.org/10.1016/j.matdes.2016.03.152.